

1 Tracking influential haze source areas in North China using 2 an adjoint model, GRAPES-CUACE

3

4 X. Q. An^{1*}, S. X. Zhai¹, M. Jin², S. L. Gong¹, Y. Wang¹

5 [1]{Chinese Academy of Meteorological Sciences, China Meteorological Administration,
6 Beijing, China}

7 [2]{Wuhan Meteorological Observatory, Wuhan, China}

8 Correspondence to: X. Q. An (anxq@cma.gov.cn)

9

10 **Abstract**

11 Based upon the adjoint theory, the adjoint of the aerosol module in the atmospheric chemical
12 modelling system GRAPES-CUACE (Global/Regional Assimilation and PrEdiction System
13 coupled with the CMA Unified Atmospheric Chemistry Environment) was developed and
14 tested for its correctness. Through statistic comparison, BC (black carbon aerosol)
15 concentrations simulated by GRAPES-CUACE were generally consistent with observations
16 from Nanjiao (one urban observation station) and Shangdianzi (one rural observation station)
17 stations. To track the most influential emission-sources regions and the most influential time
18 intervals for the high BC concentration during the simulation period, the adjoint model was
19 adopted to simulate the sensitivity of average BC concentration over Beijing at the highest
20 concentration time point (referred to as the Objective Function) with respect to BC emission
21 amount over Beijing-Tianjin-Hebei region. Four types of regions were selected based on
22 administrative division and sensitivity coefficient distribution. The adjoint model was used to
23 quantify the effects of emission-sources reduction in different time intervals over different
24 regions by one independent simulation. Effects of different emission reduction strategies
25 based on adjoint sensitivity information show that the more influential regions (regions with

1 relatively larger sensitivity coefficients) do not necessarily correspond to the administrative
2 regions, and the influence effectiveness of sensitivity-oriented regions was greater than the
3 administrative divisions. The influence of emissions on the objective function decreases
4 sharply approximately for the pollutants emitted 17~18 h ago in this episode. Therefore,
5 controlling critical emission regions during critical time intervals on the basis of adjoint
6 sensitivity analysis is much more efficient than controlling administrative specified regions
7 during an experiential time period.

8

9 **1 Introduction**

10 In the large-scale scientific and engineering calculation fields, derivative calculation exists
11 everywhere. Solving a nonlinear optimal problem requires calculating the gradient, Hessian
12 Matrix or higher-order reciprocal form (Cheng and Zhang, 2009). The traditional Finite
13 Difference Method is aimed at some basic state, changing the concerned input variable values
14 in proper order, obtaining the difference in output variables, and determining sensitivities of
15 output variables to that input variable. This method usually creates truncation errors and is
16 costly, being used only in the case of few input variables. The DDM (Decoupled Direct
17 Method), which makes use of the TLM (Tangent Linear Model), is an improvement of the
18 Finite Difference Method, but is still limited in cases of few input variables. Comparatively,
19 the adjoint method is an efficient sensitivity analysis approach, suitable for calculating the
20 parametric sensitivities of complex numerical model systems and solving various optimal
21 problems on the basis of sensitivity information. An adjoint model can work out the
22 sensitivity of every variable in each time period and each simulation grid for the objective
23 function at one simulation, which is much more efficient than the Finite Difference Method
24 and the DDM. The adjoint method is used to calculate the derivatives of meromorphic
25 functions on the basis of machine precision; thus, it has higher calculation precision and costs
26 less, being propitious to large-scale nonlinear complex calculation and playing a significant
27 role in meteorological and environmental fields. Based on the adjoint operator theory and the
28 development of numerical models, the adjoint method is applied more and more for the
29 inversion of pollution sources and other calculations that involve substantial input parameters.

1 Through this method, the tangent linear model and adjoint model of the original model can be
2 obtained on the basis of the traditional Finite Difference Method along with adjoint equation
3 theory. The principle is to build the objective function by using the difference between the
4 modelled and the observed, then to calculate the gradient (sensitivity) of the objective
5 function of to the model input parameter by using the adjoint model; this gradient can be then
6 used as a decreasing step length, correcting the input values until the objective function
7 reaches the minimum value through continuous iteration processes; therefore obtaining
8 satisfactory input parameter values (Wang, 2000).

9 The adjoint method has a unique advantage for the complex multi-parameter system. Only
10 through one simulation can it work out the sensitivity or gradient of the objective function to
11 all of the input parameters (Liu, 2005) and quickly solve various types of optimal control and
12 inversion problems by using the gradient information (Chen et al., 1998; Liu and Hu, 2003).
13 Marchuk et al. (1976, 1986) first applied the adjoint method to the atmospheric environment
14 field by using the method in the optimal control and reasonable site selection of pollution
15 sources. They cleverly utilized the conjugation property of the adjoint operator, thus avoiding
16 the pollutant transmission problems in the repeated problem-solving and greatly lessening the
17 calculation amount. Skiba et al. (2000; 2002; 2003) developed Marchuk's method and applied
18 it to solving the problems of atmospheric environment control. At present, some scientists
19 have developed adjoint models for air quality models and conducted sensitivity analyses and
20 assimilation based on these adjoint models. These adjoint models include the European air
21 pollution dispersion model of the University of Cologne, Germany (EURAD model) (Elbern
22 et al., 2000), which is mainly used in the simulation of large areas, the air quality model
23 STEM-III (Sandu et al., 2005) and the atmospheric chemical transmission model CAMx (Liu
24 et al., 2007) of the United States, etc. The adjoint of gaseous processes in CMAQ was already
25 developed, which included the chemical conversion and the transmission processes of 72
26 active species (Hakami et al., 2007). On this basis, the adjoint of the aerosol processes in
27 CMAQ will also be developed; and the CMAQ adjoint will hopefully be the first coupled
28 gas-aerosol, regional scale adjoint model to explicitly describe aerosol mass composition and
29 size distribution (Turner, 2010). Resler et al. (2010) present a version of the 4D-var

1 (four-dimensional variational) method and successfully used the adjoint of CMAQ optimized
2 diurnal profiles of NO₂ emissions. Sfetsos et al. (2013) applied the CMAQ adjoint in Athens
3 surface O₃ concentration-concentration and concentration-sources sensitivity analysis. The
4 GEOS-Chem adjoint was generated both manually and automatically and contains the
5 secondary formation processes of inorganic aerosols (Henze et al., 2007). Using the 4D-Var
6 method in the GEOS-Chem adjoint model, Henze et al. (2009) constrained emissions
7 estimates through assimilation of sulphate and nitrate aerosol measurements from the
8 IMPROVE network. Zhang et al. (2009) quantified source contributions to O₃ pollution at
9 two adjacent sites on the U.S. west coast in spring 2006 by using the GEOS-Chem chemical
10 transport model and its adjoint. García-Chan et al. (2013) utilized the adjoint method in
11 optimizing the location and management of a new industrial plant and displayed the
12 application of the adjoint method in optimal control problems. F. Paulot et al. (2014) inverse
13 modeled the NH₃ emissions in the United States, European Union, and China by using the
14 GEOS-Chem adjoint for assimilating observational data.

15 Some scientists consider the distribution of population density as well as pollutants exposure
16 – healthy reaction relationships in the objective function. For example, Pappin et al. (2013)
17 calculated health benefit influences on Canada and the United States separately from
18 emissions of individual source locations in Canada and the United States, by estimating a
19 certain reduction in anthropogenic emissions of NO_x and VOCs. Zhao et al. (2013) calculated
20 and discussed effective emissions controlling strategies under a warming climate with regards
21 to the reduction of O₃ concentration and short-term mortality due to O₃ exposure. Koo et al.
22 (2013) quantified the health risk from intercontinental pollution by using the GEOS-Chem
23 adjoint model.

24 GRAPES-CUACE is an on-line coupling of the atmospheric model GRAPES
25 (Global-Regional Assimilation and Prediction system) (Xue and Chen, 2008) and the **air**
26 **quality forecasting system** CUACE (CMA Unified Atmospheric Chemistry Environmental
27 Forecasting System) (Gong, 2003). GRAPES is a numerical weather prediction system
28 developed by Chinese scientists under the organization of the China Meteorological
29 Administration (CMA). CUACE is an air quality forecasting and climate research system

1 developed by the Chinese Academy of Meteorological Science (CAMS). In this research, the
2 adjoint model of the GRAPES-CUACE aerosol module has been developed. As the adjoint of
3 the gas-phase module and the thermodynamic equilibrium module are not available yet, only
4 BC sources and primary sources of SOAs can be tracked. The newly constructed
5 GRAPES-CUACE aerosol adjoint model was used in BC receptor-source sensitivity analysis
6 to lay the foundation of further SOAs sources (primary and secondary) tracking as well as
7 emissions inverse modelling.

8 **2 Methodology**

9 **2.1 CUACE introduction**

10 The air quality forecasting system CUACE mainly comprises 3 modules: the aerosol module,
11 the gas-phase module and the thermodynamic equilibrium module. CUACE adopted CAM
12 (Canadian Aerosol Module) (Gong et al., 2003) as its aerosol module. In this research, we
13 developed the adjoint of CAM.

14 CAM involves six types of particles, including sulphate, organic carbon, black carbon, nitrate,
15 sea-salt and soil dust, which are divided into 12 sections by using the multiphase
16 multicomponent aerosol particle size separation algorithm. The mass conservation equation of
17 the size-distributed multiphase multicomponent aerosols can be expressed as:

$$\frac{\partial X_{ip}}{\partial t} = \frac{\partial X_{ip}}{\partial t} \Big|_{TRANSPORT} + \frac{\partial X_{ip}}{\partial t} \Big|_{SOURCES} + \frac{\partial X_{ip}}{\partial t} \Big|_{CLEAR\ AIR} + \frac{\partial X_{ip}}{\partial t} \Big|_{DRY}$$
$$+ \frac{\partial X_{ip}}{\partial t} \Big|_{IN-CLOUD} + \frac{\partial X_{ip}}{\partial t} \Big|_{BELOW-CLOUD}$$

18

19 Where the rate of change of mixing ratio of dry particle mass constituent p in size range i has
20 been divided into components (or tendencies) for transport, sources, clear air, dry
21 deposition/sedimentation, in-cloud and below-cloud processes.

22 This module involves the vertical diffusion process of aerosols in the atmosphere. By solving
23 the vertical diffusion equation, the vertical diffusion trend of aerosol particles is calculated. In
24 addition, the emissions inventory is put into the module, which include both anthropogenic
25 and natural emission sources. The aerosol physical and chemical processes section is the core

1 of this module, including some primary aerosol processes in the atmosphere: aerosol emission,
 2 moisture absorption increase, collision, coagulation, condensation, dry deposition, gravity settling,
 3 sub-cloud clean-up, aerosol activation, interaction between aerosols and clouds, transmission
 4 of sulphate in clouds and clear sky.

5 **2.2 Aerosol adjoint construction and validation**

6 **2.2.1 General introduction of adjoint theory and adjoint construction**

7 Building an adjoint model for a forward model is a very complex task. To speed things up and
 8 reduce mistakes, the whole model is divided into many small programs. Abstract one small
 9 program as a vector function $F : R^n \rightarrow R^m$, which can be expressed as:

$$10 \quad Y = F(X) \quad (1)$$

11 where \mathbf{X} is a series of n-dimensional independent variables and \mathbf{Y} is m-dimensional
 12 dependent variables, representing the input variables and output variables of the original
 13 programs, respectively. Assuming that the function F is continuously differentiable at given
 14 spots of X_0 , the tangent linear model (TLM) can be expressed as:

$$15 \quad dY = \nabla_{X_0} F \cdot dX \quad (2)$$

$$\nabla_{X_0} F = \begin{pmatrix} \nabla_{X_0}^T F_1 \\ \nabla_{X_0}^T F_2 \\ \vdots \\ \nabla_{X_0}^T F_m \end{pmatrix} = \begin{pmatrix} \frac{\partial F_1}{\partial X_1} & \frac{\partial F_1}{\partial X_2} & \cdots & \frac{\partial F_1}{\partial X_n} \\ \frac{\partial F_2}{\partial X_1} & \frac{\partial F_2}{\partial X_2} & \cdots & \frac{\partial F_2}{\partial X_n} \\ \vdots & \vdots & \cdots & \vdots \\ \frac{\partial F_m}{\partial X_1} & \frac{\partial F_m}{\partial X_2} & \cdots & \frac{\partial F_m}{\partial X_n} \end{pmatrix}$$

16 where

17 Based on the mathematical formula:

$$18 \quad (LX, Y) = (X, L^*Y) \quad (3)$$

19 the adjoint expression of (2) will be:

$$20 \quad dX^* = \nabla_{X_0}^T F \cdot dY^* \quad (4)$$

1 where dX^* is of n-dimensions and dY^* is of m-dimensions. Comparing Eq. (2) with Eq. (4),
2 it is seen that these two formulas exchange dimensions between input and output with the
3 transposition of their gradient factors. Obviously, the computing cost of the tangent linear
4 model is proportional to the numbers of concerned input variables because the tangent linear
5 model requires as many calculations as the number of input variables concerned with gradient
6 information. Conversely, the adjoint model can obtain all this information through one
7 calculation. When the number of output variables is much smaller than the concerned input
8 variables, the superiority of the adjoint method is demonstrated.

9 In this study, the adjoint model was developed both manually and automatically. The
10 Automatic Differentiation Engine, TAPENADE (Tangent and Adjoint PENultimate
11 Automatic Differentiation Engine) (<http://www-tapenade.inria.fr:8080/tapenade/index.jsp>),
12 developed at INRIA Sophia-Antipolis by the TROPICS team, was used to generate the
13 tangent linear and adjoint code of sub-programs in the aerosol module CAM and of the
14 corresponding interface programs. During the adjoint generation procedure, we should
15 distinguish input variables from output variables and parameters. After that, manually
16 assembly of the divided sub-programs and the adjoint of interface programs, as well as
17 validation of the tangent linear and the adjoint models were necessary.

18 **2.2.2 Validation of tangent linear model**

19 After the adjoint model is built, its correctness must be verified to confirm its reliability. The
20 adjoint model is a concomitant of the tangent linear model (TLM). Thus, the validity of the
21 tangent linear model must be ensured before the correctness of the adjoint model is tested. If
22 all of the codes are tested as a whole, then error locations will be difficult to sense. To reduce
23 this difficulty, both the tangent linear model and the adjoint model are divided into smaller
24 sections, which are then tested separately. After these sections are confirmed, the assembled
25 TLM and adjoint model will be tested.

26 Supposing that the code of every small section is regarded as $Y = F(X)$, then the Taylor
27 expansions of $F(X + \delta X)$ at point X are:

$$1 \quad F(X + \delta X) = F(X) + \delta X F'(X) + \frac{1}{2} (\delta X)^2 F''(X) + \dots + o(\delta X)^n F^{(n)}(X) \quad (5)$$

2 After transformation:

$$3 \quad \frac{F(X + \delta X) - F(X)}{\delta X F'(X)} = 1 + \frac{1}{2} \delta X \frac{F''(X)}{F'(X)} + \dots + o(\delta X)^{n-1} \frac{F^{(n)}(X)}{F'(X)} \quad (6)$$

4 When δX approaches zero, the limit for the above equation is calculated as:

$$5 \quad Index = \lim_{\delta X \rightarrow 0} \frac{F(X + \delta X) - F(X)}{\delta X F'(X)} = 1.0 \quad (7)$$

6 In which the denominator is the TLM output, and the numerator is the difference between the
7 output value of the original model with input $X + \delta X$ and input X . To calculate the limit of
8 the above equation repeatedly, we only need to decrease δX by an equal-ratio value. If the
9 result approaches 1.0, it reflects that the tangent linear codes are correct. Generally speaking,
10 the decrease of δX causes the limit value to approach 1.0, but due to the machine rounding
11 error, the limit values might decrease first and then increase, appearing as a parabola. The
12 validation results are displayed in Table 1.

13 **2.2.3 Validation of the adjoint model**

14 After all of the tangent linear codes have passed the testing, the adjoint codes can then be
15 tested on this basis. The adjoint codes and tangent linear codes need to satisfy Eq. (3):

$$16 \quad (L(X), Y) = (X, L^*(Y))$$

17 In which L represents the tangent linear process and L^* the adjoint process. To simplify the
18 testing process, the adjoint input is set as the tangent linear output: $Y = L(X)$. Then, the
19 above equation can be expressed as:

$$20 \quad (\nabla F \bullet dX, \nabla F \bullet dX) = (dX, \nabla^T F (\nabla F \bullet dX)) \quad (9)$$

21 By putting dX into the tangent linear codes, the output value $\nabla F \bullet dX$ can be obtained and the
22 left part of the equation can be computed. Then, taking $\nabla F \bullet dX$ as the input of the adjoint
23 codes, we obtain its output value $\nabla^T F (\nabla F \bullet dX)$ and then calculate the right part of the

1 equation. As long as the result of the equation is approximately equal (within the error range),
2 the constructed adjoint model is considered to have passed the validation. The validation
3 results of pollutant concentration variable $xrow$ are shown in Table 2.

4 Seen from Table 2, both sides of the equation have produced values with 14 identical
5 significant digits or more. This result is within the range of computer errors, so the values of
6 the left and the right sides are considered to be equal, so the pollutant concentration variable
7 $xrow$ has passed the adjoint testing. Due to limited space, only the adjoint testing result of
8 $xrow$ is presented here. In fact, when performing the actual validations, all of the parameters
9 are tested, respectively; although some parameters only have 11-12 identical significant digits,
10 indicating lower precision, they are still considered to be within the permitted scope. Till now,
11 all of the model variables have passed the adjoint testing.

12 **2.2.4 Assembly and operation flow of GRAPES-CUACE aerosol adjoint**

13 After each part and the assembled TLM and adjoint model have been verified, the
14 GRAPES-CUACE aerosol adjoint model is constructed. The structures and parameters
15 passing flowchart are shown in Fig. 1. In Fig. 1, ADJ is short for adjoint; X_n , X_{n+1} represent
16 model parameters after n , $n+1$ GRAPES-CUACE integral time steps, respectively; X_n^* , X_2^*
17 represent, correspondingly, X_n 's adjoint $\partial J / \partial X_n$ and X_2 's adjoint $\partial J / \partial X_2$, where J is the
18 objective function; $\partial J / \partial X$ are forcing terms; structures and variables in solid line frames are
19 related to forward simulation; structures and variables in dashed frames are adjoint simulation
20 relevant. In addition, as GRAPES-CUACE is an on-line meteorological chemistry modelling
21 system, the aerosol transport processes are extracted from GRAPES, therefore, a process
22 called "aerosol-related transport adjoint" is in Fig.1.

23 When operating, the forward GRAPES-CUACE should be run first to save basic state values
24 of un-equilibrated variables in checkpoint files. Intermediate values are recalculated or saved
25 in stack during the adjoint integration. Then, the saved basic state values during the forward
26 integration and the forcing terms are used as inputs in the adjoint backward simulation.

1 2.3 Sensitivity analysis

2 To conduct sensitivity analysis and solve environmental optimization problems, we tend to
3 take into account various factors, including air quality standard, economic loss, health benefit,
4 emissions reduction enforceable ratios range, suitable locations for factories, etc. Hence, a
5 reasonable evaluation function J is needed, which includes one or several of the above factors
6 as independent variables or/and as controlling conditions. In the adjoint method, such a
7 function is called the objective function. We can define various types of objective functions
8 based on different purposes. An objective function is always a simple function of output
9 parameters (e.g., $J=J(Y)$) compared with a complex atmospheric chemistry modeling system
10 $Y=F(X)$.

11 The adjoint input, also called the forcing term (Fig. 1), is the gradient of J with respect to
12 model output Y : $\nabla_Y J$, which is relatively easy to obtain. The adjoint output, also called aiming
13 sensitivity information, is the gradient of J with respect to any model parameter X : $\nabla_X J$. To
14 endow a definite physical meaning to sensitivity information, we define the sensitivity
15 coefficient as the product of one model parameter X and $\nabla_X J$: $X * \nabla_X J$. This sensitivity
16 coefficient has the same unit as the objective function J .

17 When controlling a severe pollution event, J is often defined as the concentration of a
18 concerned pollutant at the time with the most serious pollution. Then, the inverse adjoint
19 method can be used to locate where and when the emissions should have the
20 greatest influence.

21 In emission inventory optimization problems, J is often defined as the discrepancy between
22 the simulated and observed values. Running the adjoint model once, the gradients (sensitivity)
23 of the objective function to emission amount can be obtained, and then, by using the gradient
24 information iteratively, the optimal solution of the objective function is determined. In this
25 adjoint sensitivity analysis research, we use the adjoint method to locate the most influential
26 emission sources regions and the most influential emission time periods.

1 **2.4 Model setup**

2 In this study, the GFS reanalysis data, which are collected 6 times a day with $1^\circ \times 1^\circ$ resolution,
3 are used for initial and boundary conditions in the GRAPES-CUACE modeling system, and
4 INTEX-B2006 ($0.5^\circ \times 0.5^\circ$) is used as the emission sources. With a horizontal resolution of
5 $0.5^\circ \times 0.5^\circ$, the simulation domain covers Northeast China (105°E - 125°E , 32.25°N - 42.25°N),
6 as shown in Fig. 2. Our analysis mainly focuses on the Beijing-Tianjin-Hebei (BTH) region.
7 The entire simulation period is from 20:00 BT (Beijing Time) 28 June 2008 to 20:00 BT 4
8 July 2008, and the first 72 h are regarded as the spin-up time.

9 **2.5 Observations**

10 The data used in this paper are hourly black carbon aerosol (BC) average concentrations from
11 the Beijing Meteorological Observatory Nanjiao Station and Shangdianzi Station. The
12 Nanjiao Station (39.8°N , 116.47°E) is located in the Atmospheric Observation Test Base in
13 the southern suburb of Beijing. It is next to the Beijing urban area in the north and close to
14 Fifth Ring Road in the south, where traffic flows are relatively large. The Shangdianzi Station
15 (40.65°N , 117.12°E) is at the Shangdianzi village of Miyun County in northeastern Beijing.
16 This station is a regional atmospheric background station, around which there is no obvious
17 industrial pollution and few human activities, i.e., it has a better ecological environment. The
18 locations of the two stations are shown in Fig. 2.

19 **3. Results and discussion**

20 BC is an important component of atmospheric aerosols. It is emitted directly into the
21 atmosphere predominantly during combustion (Seinfeld, 2006). Its sources include
22 anthropogenic and natural emission sources. Natural sources (e.g., volcanic eruption and
23 forest fires) are occasional and regional, contributing little to the long-term background BC
24 concentration in the atmosphere (Nagamoto et al., 1993). Comparatively, many human
25 activities increase the concentration of the BC aerosols; so anthropogenic sources are the
26 primary sources for BC. Cao et al. (2006) and Streets et al. (2001) noted that the vast majority
27 of BC emission in China is created by the untreated raw coal, honeycomb briquettes, and
28 biomass fuels that people use in their daily lives.

1 BC is the main light absorbing aerosol species; it alters the radiative properties of other
2 aerosols with which it is mixed. In addition, it may also affect cloud formation and
3 precipitation (Hakami, 2005), reduce crop production, decrease visibility, as well as harm
4 human health. In one word, BC plays an essential role in atmospheric radiative forcing,
5 climate change and air quality evaluation.

6 **3.1 High BC concentration episode and model validation**

7 The simulated ground BC concentration distributions from 20:00 BT July 3 to 11:00 BT July
8 4 are shown in Fig. 3. These six graphs demonstrate the formation and transportation
9 processes of this high BC concentration episode over Beijing. At 20:00 BT 3 July, two small
10 spots of high BC concentration appear around Shijiazhuang and southern Beijing. Then, at
11 23:00 BT 3 July, these two high BC concentration spots are obviously enlarged, and are
12 almost connected, extending to northern Xingtai, eastern Baoding, Langfang and Tianjin. At
13 2:00 BT 4 July, high BC concentration area develops around Beijing, Tianjin, southern Hebei
14 and the Henan province. Then, it gets enlarged and intensified continuously during the
15 subsequent hours until 11:00 BT 4 July, when the influenced scope begins to narrow due to
16 enhanced dispersion and vertical movement in the boundary layer. However, the BC
17 concentration over Beijing still remains at a relatively higher level.

18 Fig. 4 shows hourly variation of ground level BC concentration in Beijing. It is easy to notice
19 that during the first 2 simulated days, the BC concentration value reaches its peak at
20 approximately 2:00 BT 2 and 3 July and its lowest value at approximately 15:00 BT. This
21 result is closely affected by the diurnal height variation of the boundary layer, atmospheric
22 stability and diffusion conditions. Different from the previous 2 days, the highest BC
23 concentration value on 4 July, i.e., $15.7 \mu\text{g}/\text{m}^3$, occurs at 11:00 BT. This might be because, on
24 4 July, the atmospheric condition is more stable and the pollutant diffusion condition is
25 unsatisfactory, thus leading to BC accumulation.

26 The model results are compared with observation data in Fig. 5. The correlation coefficients
27 of the simulated and the observed BC concentrations at Shangdianzi and Nanjiao station are
28 0.65 and 0.54, respectively. So the general variation trends of the simulated and observed BC

1 concentrations are consistent, except that the simulated BC concentration values are bigger
2 than the corresponding observed ones. Overall, the model results are acceptable.

3 **3.2 Objective function and sensitivity coefficient definitions**

4 As mentioned above, the adjoint method can provide information about influences of
5 location-specific sources on the function called “objective function”. To determine the area
6 and time period of the most important emission sources that induce the high BC concentration
7 over Beijing at 11:00 BT 4 July 2008 (Fig. 4), we define the objective function J as average
8 BC concentration over Beijing at 11:00BT 4 July 2008.

9 The adjoint input, also regarded as the forcing term, is $\partial J/\partial C$. C represents the pollutant
10 concentration, such as BC concentration, at the objective time point. The direct output from
11 the adjoint model is the gradient of J with respect to any model parameter var: $\partial J/\partial \text{var}$. If Q is
12 emission intensity, we define the emission sensitivity coefficient Φ as:

$$13 \quad \Phi = Q \frac{\partial J}{\partial Q}$$

14 In this way, the emission sensitivity coefficient Φ has the same unit with J and has a specific
15 physical meaning. The bigger the sensitivity coefficient value is, the larger the influence of
16 BC emission in that area has on J . If BC emission is cut by $N\%$, the value of J will decrease
17 by $N\%*\Phi$, which means that the average BC concentration over Beijing at the objective time
18 point will decrease by $N\%*\Phi$.

19 **3.3 Distribution of adjoint sensitivity**

20 When controlling air quality by cutting down emissions, we tend to cut emissions over a
21 certain period of time, e.g., starting to cut emissions 1-3 days ahead of the predicted severe
22 pollution day. Based on this practical concept, sensitivity coefficients at every model
23 backward integral time step are added from the objective time point (highest BC
24 concentration: 11:00 BT 4 July 2008) to a certain preceding time point, as illustrated in Fig. 6.
25 Figure 6 shows a spatial-temporal cumulative effect from BC emissions to the objective
26 function J .

1 As shown in Fig. 6, sensitivity coefficients accumulate along an inverse time series. When
2 sensitivity coefficients from the previous 1 h until the objective time point are added, only the
3 Tongzhou and Daxing districts in Beijing have sensitivity coefficients of 0.05-0.1 $\mu\text{g}/\text{m}^3$.
4 When sensitivity coefficients are added during the last 6 h, the influential area is remarkably
5 enlarged, with a maximum value of 0.3-0.4 $\mu\text{g}/\text{m}^3$. As the hours ahead of the objective time
6 points considered extend, this influenced area is continually enlarged and intensified. When it
7 reaches the 16-h period of time, as shown in Fig. 6(d), the more critical area expands to
8 Langfang and Baoding of Hebei province, and the maximum value is approximately 0.7
9 $\mu\text{g}/\text{m}^3$, which indicates that reducing BC emission at the ratio of $N\%$ from 19:00 BT 3 July to
10 the objective time point over this grid cell could result in about an average $N\%*0.7 \mu\text{g}/\text{m}^3$
11 decrease of BC concentration over Beijing, the objective region, at 11:00 BT 4 July 2008, the
12 objective time point. However, along with this accumulation procedure, the expansion of the
13 influential region scope and the increase of its sensitivity coefficients begin to slow down.
14 Only a tiny difference between 24 h of accumulation (Fig. 6 (f)) and 48 h of accumulation
15 (Fig. 6 (g)) is observed. This phenomenon reflects that emissions at a very early time, such as
16 more than 24 h ahead of the objective time point, have little influence on J . When a heavy
17 pollution event needs to be controlled by reducing emissions, the time period with most
18 significant influence should be scientifically determined to cut emissions both effectively and
19 economically.

20 **3.4 Time series of sensitivity coefficients over different regions**

21 Adjoint sensitivity analysis is a powerful compliment to forward methods. While forward
22 techniques are source-based, backward methods provide receptor-based sensitivity
23 information. Under this conception, we use the adjoint method to locate the most influential
24 emission sources area and the most influential emission time period.

25 Four types of regions are defined according to administrative division and sensitivity
26 coefficients distribution (Table 3 and Fig. 7). BTH refers to the administrative
27 Beijing-Tianjin-Hebei region, which covers 105 grid cells and is approximately 318,000 km^2 ;
28 BJ represents administrative Beijing, which contains 10 grid cells and covers an area of

1 around 30,000 km². InR-1 (Influential Region 1) has 7 grid cells, occupying about 21,000 km²,
2 which is smaller than that of BJ, whose sensitivity coefficient values are obviously bigger
3 than others; InR-2 (Influential Region 2) covers InR-1 and 10 more grid cells with secondary
4 large coefficient values, having 17 grid cells in total and covering approximately 51,000 km².

5 To compare the effects of emission-sources reduction at different time points in the 4 regions,
6 we add BC emission sensitivity coefficients vertically and extract their inverse time series
7 values (Fig. 8). Fig. 8 (a) is the inverse time series of sensitivity coefficients at every 5-min
8 integration time step. It reflects the influence of BC emission on the objective function J at
9 each model integration time step ahead of the objective time point. Fig. 8 (b) shows the time
10 cumulative sensitivity coefficients, which reveal the decrease of J due to BC emission
11 reduction over a certain period of time ahead of the most polluted time point.

12 In Fig. 8 (a), the sensitivity coefficients of BTH, InR-1 and BJ reach their peak values at
13 18:00 BT 3 July, while that InR-2 at 17:00 BT 3 July, and then all decrease sharply along
14 backward time sequence. This phenomenon indicates that emissions emitted 17~18 h before
15 the most serious pollution time point have rapid decreasing effects on J along the inverse time
16 sequence axis. Correspondingly, in Fig. 8 (b), the time cumulative sensitivity coefficients
17 obviously slow down their increasing trend at 18:00 BT 3 July. This phenomenon shows that
18 cutting emissions before the predicted pollution episode can have better effects on air quality
19 control than doing so after severe pollution events occur. In addition, it also shows that the
20 emission reduction start-up time point should be scientifically determined based on adjoint
21 sensitivity or other information to increase the efficiency of air quality control.

22 Then we compared the preceding 18-hr, 17:00 BT 3 July to 11:00 BT 4 July, cumulative
23 sensitivity coefficients of the above 4 regions (Table 4), given it that the sensitivity coefficient
24 on 17:00 BT 3 July is still relatively high (for BTH, InR-1, and BJ). From Table 4, the
25 simulated SC (sensitivity coefficient) of BTH is 7.3 $\mu\text{g}/\text{m}^3$, meaning that a reduction of $N\%$
26 BC emissions over BTH will cause an $N\%*7.3\mu\text{g}/\text{m}^3$ decrease of average BC concentration in
27 Beijing on 11:00 BT 4 July. In general, it is obvious that reducing emissions over the whole
28 BTH region will contribute most positively to air quality control in Beijing, followed by
29 InR-2, InR-1 and BJ respectively. However, in the 4 regions, the SC/Grid (sensitivity

1 coefficient per grid) value of InR-1 is the largest, meaning cutting emissions of InR-1 has the
2 most obvious effectiveness on decreasing BC concentration in Beijing. The SC/Grid of BTH
3 is the smallest, and InR-2 equals BJ in between. BTH covers an area which is 6.2 times that of
4 InR-2, but the SC and SC/Grid of Inr-2 are 80% and 5.0 times of BTH (Table 4). A similar
5 phenomenon is found between BJ and InR-1. InR-1 accounts for only 70% of the area of BJ,
6 but the SC and SC/Grid of InR-1 are 1.2 and 1.6 times of BJ.

7 **4. Conclusions**

8 On the basis of adjoint theory and methods, this paper has constructed an adjoint model for an
9 aerosol module of the atmospheric chemical model GRAPES-CUACE and tested the
10 correctness of the model. At the same time, the GRAPES-CUACE model and its aerosol
11 adjoint were adopted to perform a numerical simulation and a receptor-source sensitivity test.
12 Compared with the BC aerosol observations from the Nanjiao and Shangdianzi stations, the
13 hourly trends of BC concentration were similar, with correlation coefficients of 0.65 and 0.54,
14 respectively.

15 The GRAPES-CUACE adjoint model simulated the sensitivity of concentration on emission
16 and was adopted to track the most influential emission-sources regions and most influential
17 time intervals for the high BC concentration. Four types of regions were selected and
18 compared based on administrative division and adjoint sensitivity coefficient distribution. The
19 result of the aerosol adjoint model suggested that the influence effectiveness of
20 sensitivity-oriented regions was greater than the administrative divisions. For the case studied
21 in this paper, emissions from 17~18 h ahead of the objective time point had a much larger
22 influence than emissions emitted earlier.

23 **Through analysing the result of BC adjoint sensitivity results, it's naturally to shine light on**
24 **designing efficient haze control schemes using the adjoint method.** It is found that in order to
25 increase emission reduction efficiency, influential regions should be located scientifically (e.g.,
26 according to adjoint sensitivity coefficients distribution) rather than by administrative
27 divisions.

28 **Code availability**

1 We use the GRAPES-CUACE as distributed by Numerical Weather Prediction Center of
2 Chinese Meteorology Administration (<http://nwpc.cma.gov.cn>) together with Institute of
3 Atmospheric Composition of Chinese Academy of Meteorological Sciences
4 (<http://cadata.cams.cma.gov.cn>). The model runs on IBM PureFlex System (AIX) with XL
5 Fortran Compiler. The CUACE-ADJ code can be requested from the corresponding author or
6 downloaded as a Supplement to this article.

7 **Acknowledgements**

8 This study was supported by the National Basic Research Program of China “973”
9 (2011CB403404), and partially supported by the CMA Innovation Team for Haze-fog
10 Observation and Forecasts. We appreciate Lin Zhang, Feng Liu, Qiang Cheng, Hongliang
11 Zhang and Min Xue for providing technical support in adjoint model construction. Thanks
12 also to the developers of the GRAPES-CUACE aerosol model.

13

14 **References**

15 Cao, G., Zhang, X., Wang, Y., Che, H., and Chen D: Inventory of Black Carbon Emission
16 from China, *Advances in Climate Change Research*, 2 (6): 259-264, 2006. (In Chinese)

17 Cao, G., Zhang, X., Gong, S., An, X. and Wang, Y.: Emission inventories of primary particles
18 and pollutant gases for China. *Chinese Sci Bull*, 56(03): 261-268, 2011.

19 Chen, H., Hu, F., Zeng, Q. and Chen, J.: Some Practical Problems of Optimizing Emissions
20 from Pollution Sources in Air, *Climatic and Environmental Research*, 3(2): 163-172, 1998.
21 (In Chinese)

22 Cheng, Q., Zhang, H. and Wang, B.: Algorithms of Automatic Differentiation, *Mathematica*
23 *Numerica Sinica*, 33(1):15-36, 2009. (In Chinese)

24 Elbern, H., Schmidt, H., Talagrand, O. and Ebel, A.: 4D-variational data assimilation with an
25 adjoint air quality model for emission analysis. *Environmental Modelling & Software*,
26 15:539-548, 2000.

1 Garc ía-Chan, N., Alvarez-V ázquez, L., Mart ínez, A., and V ázquez-M éndez, M.: On optimal
2 location and management of a new industrial plant: Numerical simulation and control, Journal
3 of the Franklin Institute, 2013.

4 Gong, S. L., Barrie, L. A., Blanchet, J.-P., Salzen, K. v., Lohmann, U., Lesins, G., Spacek, L.,
5 Zhang, L. M., Girard, E., and Lin, H.: Canadian Aerosol Module: A size-segregated
6 simulation of atmospheric aerosol processes for climate and air quality models, 1, Module
7 development (DOI 10.1029/2001JD002002), Journal of geophysical research, 108, 2003.

8 **Hakami, A., Henze, D. K., and Seinfeld, J. H.: Adjoint inverse modelling of black carbon**
9 **during the Asian Pacific Regional Aerosol Characterization Experiment, Journal of**
10 **Geophysical Research, Vol. 110, D14301, doi: 10.1029/2004JD005671, 2005.**

11 Hakami, A., Henze, D. K., Seinfeld, J. H., Singh, K., Sandu, A., Kim, S., Byun, D., and Li, Q.:
12 The adjoint of CMAQ, Environmental science & technology, 41, 7807-7817, 2007.

13 Henze, D., Hakami, A., and Seinfeld, J.: Development of the adjoint of GEOS-Chem, Atmos.
14 Chem. Phys., 7, 2413-2433, 2007.

15 Henze, D., Seinfeld, J., and Shindell, D.: Inverse modeling and mapping US air quality
16 influences of inorganic PM 2.5 precursor emissions using the adjoint of GEOS-Chem, Atmos.
17 Chem. Phys., 9, 5877-5903, 2009.

18 **Seinfeld, J. H. and Pandis S. N.: Atmospheric Chemistry and Physics: From Air Pollution to**
19 **Climate Change, Second Edition, John Wiley & Sons, Inc., pp. 628-633.**

20 Koo, J., Wang, Q., Henze, D. K., Waitz, I. A., and Barrett, S. R.: Spatial sensitivities of
21 human health risk to intercontinental and high-altitude pollution, Atmos. Environ., 2013.

22 Liu, F., Hu, F.: Inversion of Diffusion on Coefficients And Effect of Related Difference
23 Schemes, Journal of Applied Meteorological Science, 14(3):331-338, 2003. (In Chinese)

24 Liu, F.: Adjoint model of Comprehensive Air quality Model CAMx – construction and
25 application, Peking University Post-doctoral Research Report, 2005.

26 Liu, F., Zhang, Y., Su, H., Hu, J.: Adjoint Model of Atmospheric Chemistry Transport Model
27 CAMx: Construction and Application, Acta Scientiarum Naturalium Universitatis Pekinensis,
28 43(6): 764-770, 2007. (In Chinese)

1 Marchuk, G., Skiba, Y.: Numerical calculation of the conjugate problem for a model of the
2 thermal interaction of the atmosphere with the oceans and continents. *Izvestiya Atmospheric*
3 *Oceanic Physics*, 12: 279-284, 1976.

4 Marchuk, G.: *Mathematical Models in Environmental Problems*, New York: Elsevier Science
5 Publishers, 1986.

6 Nagamoto, F., Zhou, M.: Aeolian transport of aerosol black carbon from China to the ocean.
7 *Atmos. Environ.*, 28(20) : 3251-3260, 1994.

8 Pappin, A. J., and Hakami, A.: Source Attribution of Health Benefits from Air Pollution
9 Abatement in Canada and the United States: An Adjoint Sensitivity Analysis, *Environmental*
10 *Health Perspectives*, 121, 572, 2013.

11 Paulot, F., Jacob, D. J., Pinder, R. W., Bash, J. O., Travis, K., and Henze, D. K.: Ammonia
12 emissions in the United States, European Union, and China derived by high-resolution
13 inversion of ammonium wet deposition data: Interpretation with a new agricultural emissions
14 inventory (MASAGE_NH3), *Journal of Geophysical Research: Atmospheres*, 2014.

15 Resler, J., Eben, K., Jurus, P., and Liczki, J.: Inverse modeling of emissions and their time
16 profiles, *Atmospheric Pollution Research*, 2010.

17 Sandu, A., Daescu, D. N., Carmichael, G. R., and Chai, T.: Adjoint sensitivity analysis of
18 regional air quality models, *Journal of Computational Physics*, 204, 222-252, 2005.

19 Sfetsos, A., Vlachogiannis, D., and Gounaris, N.: An Investigation of the Factors Affecting
20 the Ozone Concentrations in an Urban Environment, *Atmospheric and Climate Sciences*, 3,
21 11-17, 2013.

22 Skiba, Y. and Parra-Guevara D.: Industrial pollution transport. Part 1. Formulation of the
23 problem and air pollution estimates. Part 2. Control of industrial emissions. *Environmental*
24 *Modeling and Assessment*, 2000. 5:169-175, 177-184.

25 Skiba Y N, and Davydova-Belitskaya V.: Air pollution estimates in Guadalajara City.
26 *Environmental Modeling and Assessment* .2002.7: 153~162.

27 Skiba Y N and Davydova-Belitskaya V.: On the estimation of impact of vehicular emissions.
28 *Ecological Modelling* 2003. 166:169-184.

1 Streets, D., Gupta, S., Waldho, S.: Black carbon emissions in China. *Atmos. Environ.*, 35:
2 4281-4296, 2001.

3 Turner, M.: Inverse Modeling of NO_x and NH₃ Precursor Emissions Using the Adjoint of
4 CMAQ, Research Prelim Report, Department of Mechanical Engineering, University of
5 Colorado, 2010.

6 Wang, X: Toward the Objective Analysis, Four-Dimensional Assimilation and Adjoint
7 Method, *Journal of PLA University of Science and Technology*, 1(2): 67-74, 2000. (In
8 Chinese)

9 Xu, L., Wang, Y., Chen, Z., Luo, Y. and Ren, W.: Progress of Black Carbon Aerosol
10 Research I :Emission , Removal and Concentration, *Advances in Earth Science*,
11 21(6):352-359, 2006. (In Chinese)

12 Xue, J., Chen, D.: Scientific Design and Application of Numerical Predicting System
13 GRAPES, Science Press, Beijing, 2008

14 Yin, Y., Cui, Z., Zhang, H.: Numerical Simulations of Mass Distribution of Aerosol over
15 China in 2006, *Transactions of Atmospheric Sciences*, 32 (5) : 595-603, 2009. (In Chinese)

16 Zhang, L., Jacob, D. J., Kopacz, M., Henze, D. K., Singh, K., and Jaffe, D. A.:
17 Intercontinental source attribution of ozone pollution at western U.S. sites using an adjoint
18 method, *Geophysical Research Letters*, 36, L11810, 10.1029/2009gl037950, 2009.

19 Zhao, S., Pappin, A. J., Morteza Mesbah, S., Joyce Zhang, J., MacDonald, N. L., and Hakami,
20 A.: Adjoint estimation of ozone climate penalties, *Geophysical Research Letters*, 40,
21 5559-5563, 2013.

22 Zhu, J., Zeng, Q., Guo, D., and Liu, Z: Optimal control of Sedimentation in Navigation
23 Channels, *Journal of Hydraulic Engineering*, 125(7):750-759, 1999.

24 Zhu, J. and Zeng, Q.: A mathematical theory frame for atmospheric pollution control, *Science*
25 *China (D)*, 32(10):864-870, 2002.

26

1

Table 1. Validation results of tangent linear model.

a	Index (xrow)	Index (rhop)
1.00000000000	0.961383789	1.064836676
0.10000000000	0.996231252	1.005283209
0.01000000000	0.999622785	1.000526942
0.00100000000	0.999962182	1.000052673
0.00010000000	0.99999532	1.000005301
0.00001000000	0.999995319	1.000000848
0.00000100000	0.999974073	1.000001471
0.00000010000	0.998912182	1.000034692
0.00000001000	0.996789129	1.000189939
0.00000000100	0.913747381	1.002300501

2

3

1

Table 2. Validation results of adjoint model.

Integral step	VALTGL	VALADJ
1	0.253071834334799587E-11	0.253071834334799587E-11
2	0.138781684963437701E-07	0.138781684963437635E-07
3	0.197243288646595624E-06	0.197243288646595703E-06
4	0.285995663142418833E-06	0.285995663142418833E-06
5	0.138094513716334626E-06	0.138094513716334599E-06
6	0.158774915826234477E-06	0.158774915826234609E-06
7	0.205383106884893541E-06	0.205383106884893673E-06
8	0.113356629291541069E-06	0.113356629291540963E-06
9	0.151566991405230902E-06	0.151566991405230823E-06
10	0.174929034468917025E-06	0.174929034468917104E-06
11	0.333573941572600298E-06	0.333573941572600616E-06
12	0.185912861066765391E-06	0.185912861066765523E-06

2

3

1

Table 3. Information of 4 emission reduction regions

Region	Number of Grid cells	Area(km ²)
BTH	105	318000
BJ	10	30000
InR-1	7	21000
InR-2	17	51000

2

3

1 Table 4. 18-hr (17:00 BT 3 July - 11:00 BT 4 July) cumulative SC and SC/Grid over 4
 2 emission reduction regions

3

Regions	BTH	BJ	InR-1	InR-2	InR-2/BTH	InR-1/BJ
SC	($\mu\text{g}/\text{m}^3$)	($\mu\text{g}/\text{m}^3$)	($\mu\text{g}/\text{m}^3$)	($\mu\text{g}/\text{m}^3$)		
SC	7.3	3.5	4.0	5.9	0.8	1.2
SC/Grid	0.07	0.35	0.58	0.35	5.0	1.6

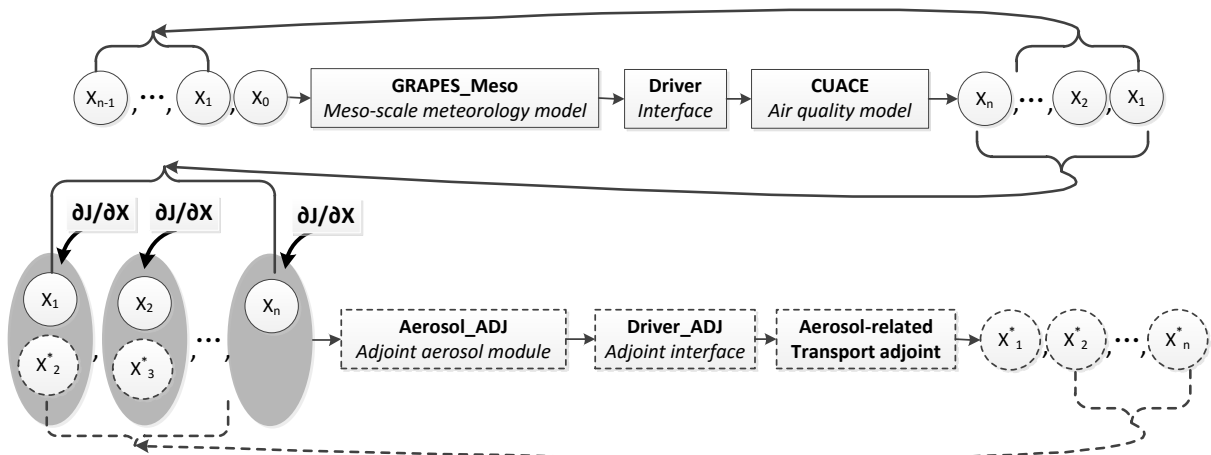
4 SC: Sensitivity coefficient

5 SC/Grid: Sensitivity coefficient per simulation grid

6

1

2

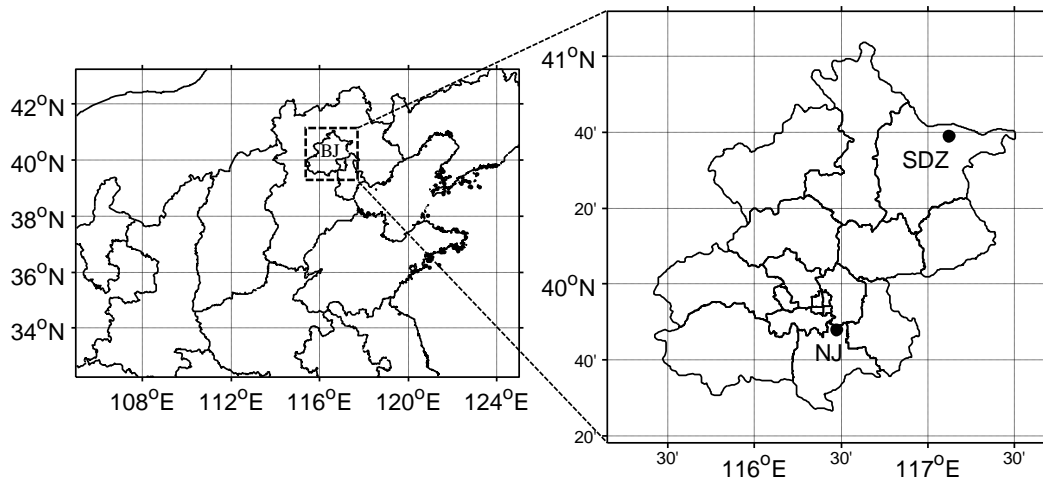


3

4 Figure 1. Frame work of GRAPES-CUACE, **aerosol adjoint** and the flowchart of parameters
5 transmission

6

7



1
2
3
4

Figure 2. Left: model domain settings (left); right: the locations of Nanjiao (NJ) and Shangdianzi (SDZ) observation sites.

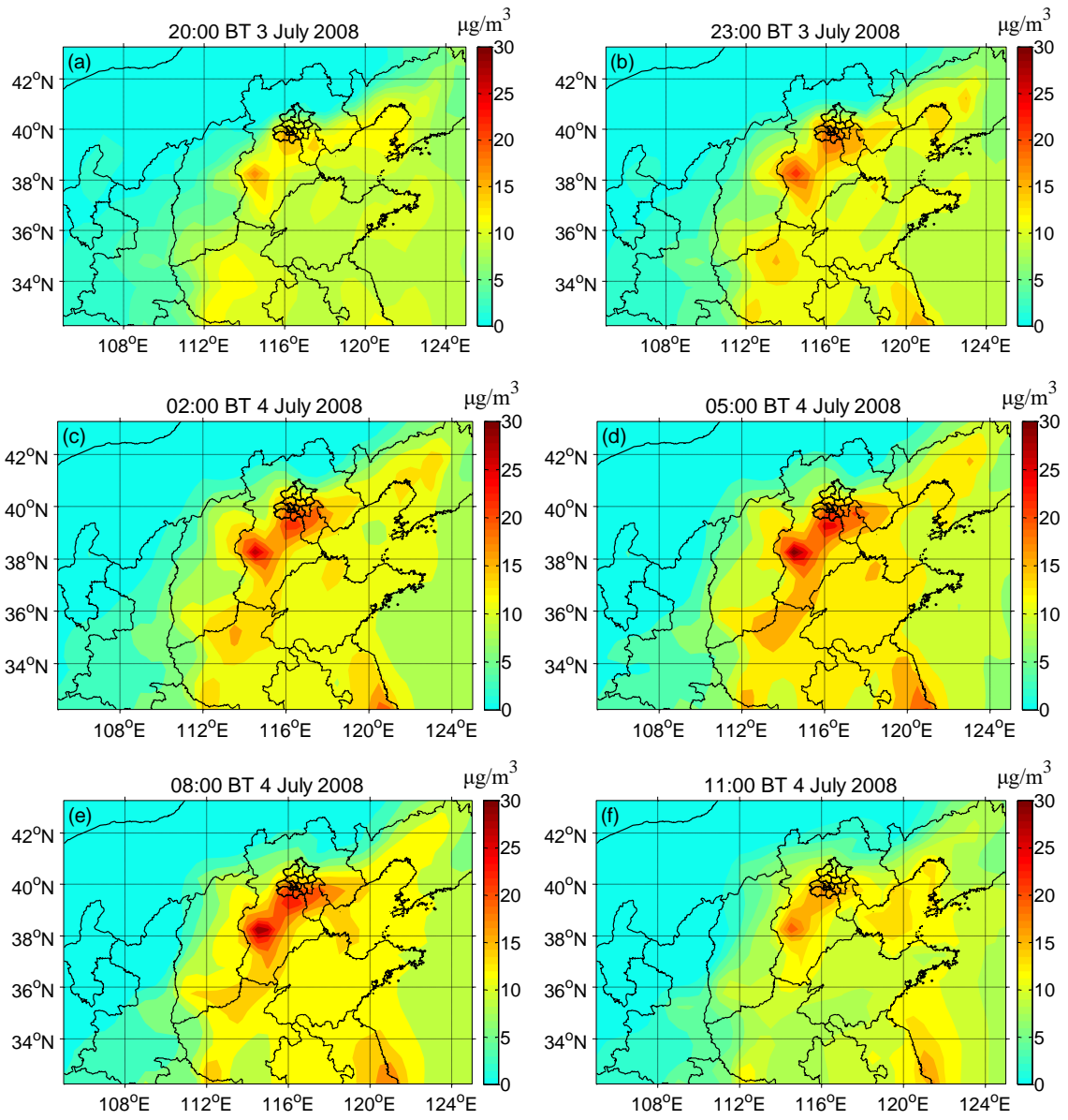


Figure 3. BC concentration distribution at ground level (Unites: $\mu\text{g}/\text{m}^3$).

1

2

3

4

5

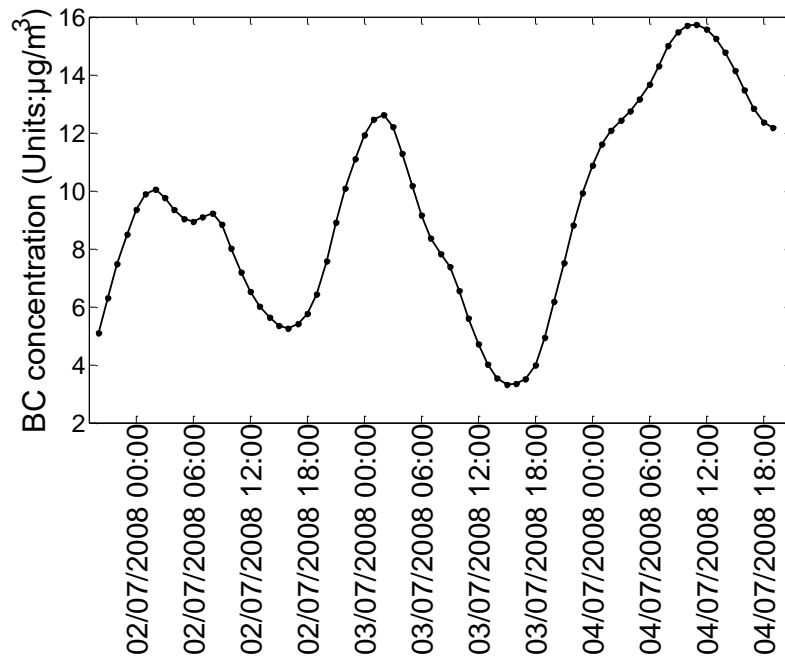
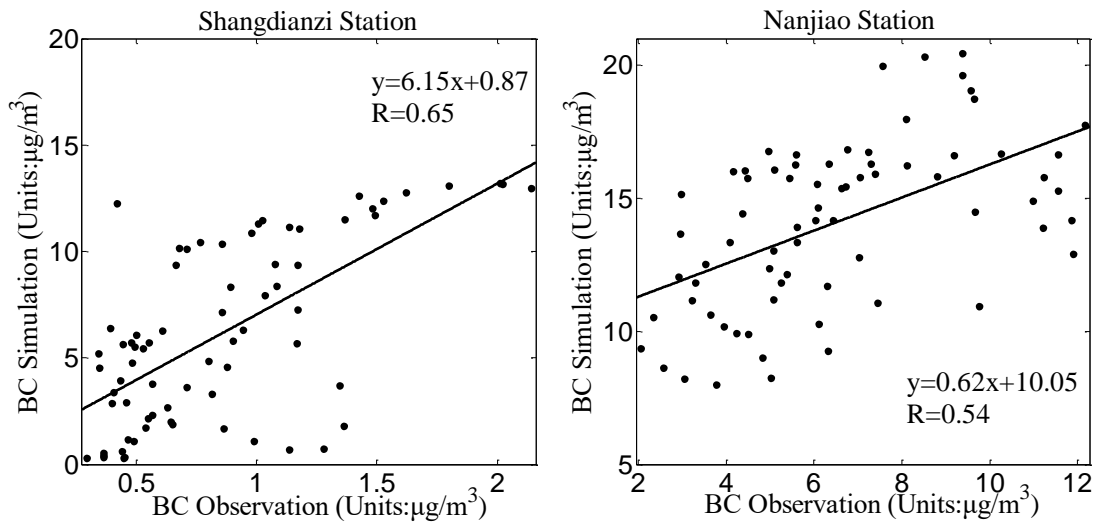


Figure 4. Hourly variation of ground BC concentration in Beijing.

1
2
3



1
2
3
4
5

Figure 5. Correlation coefficients of simulated and observed BC concentration at Shangdianzi and Nanjiao Station.

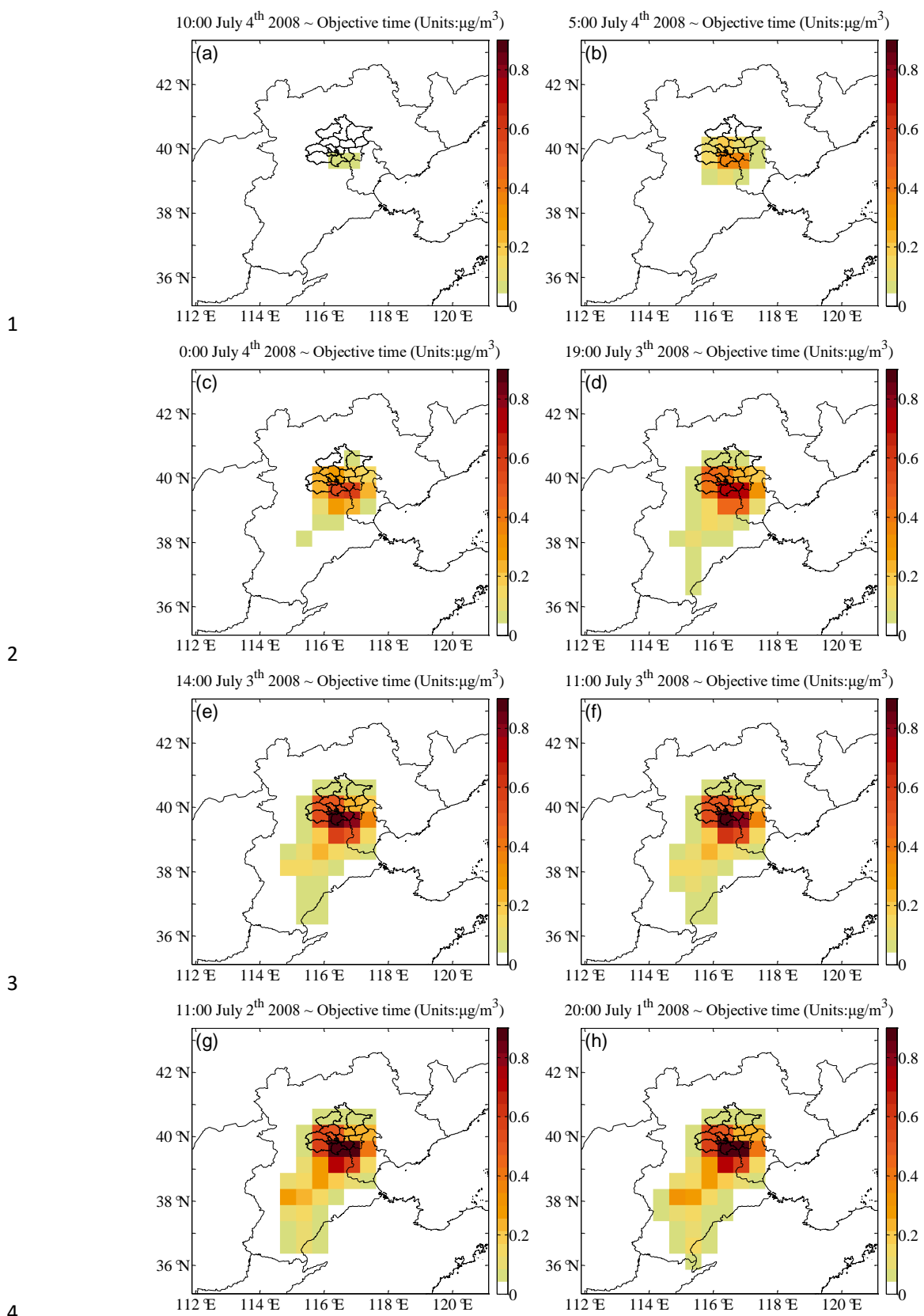
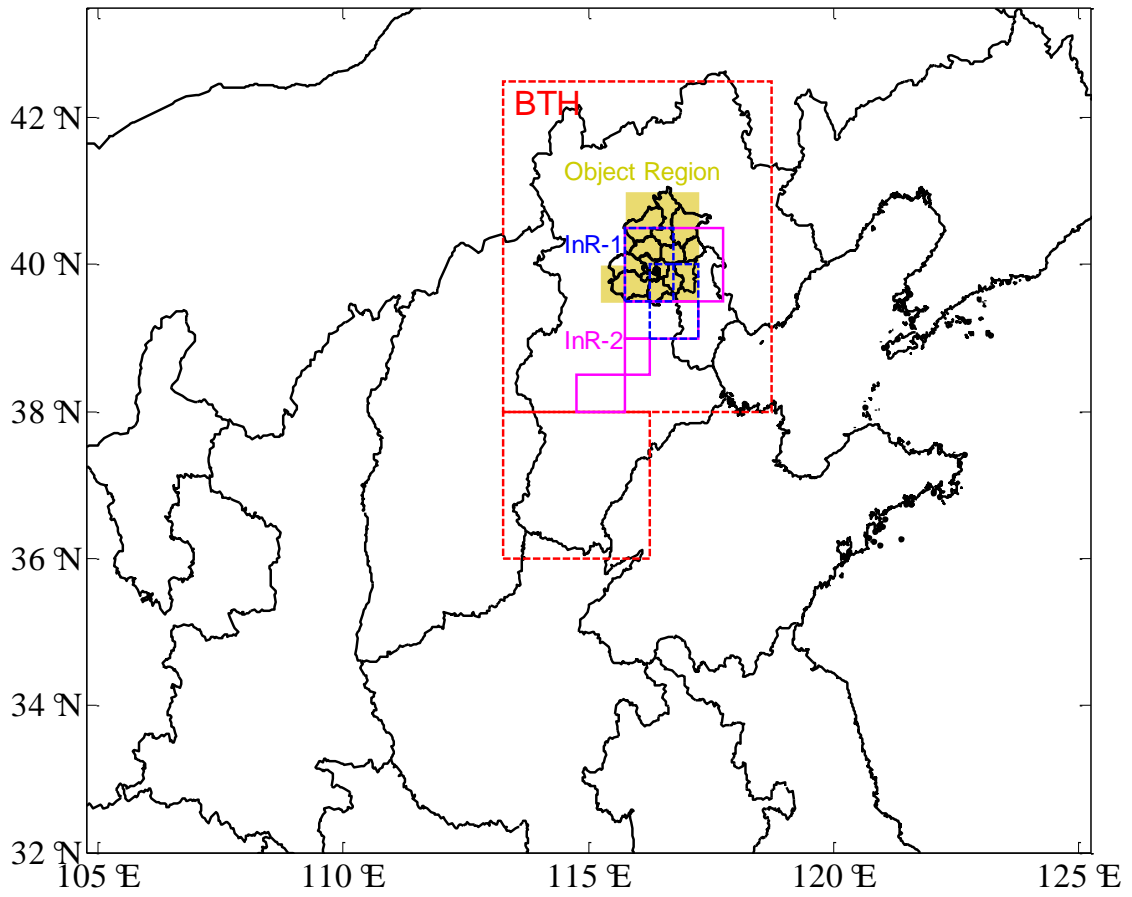


Figure 6. Cumulative sensitivity coefficient distribution.

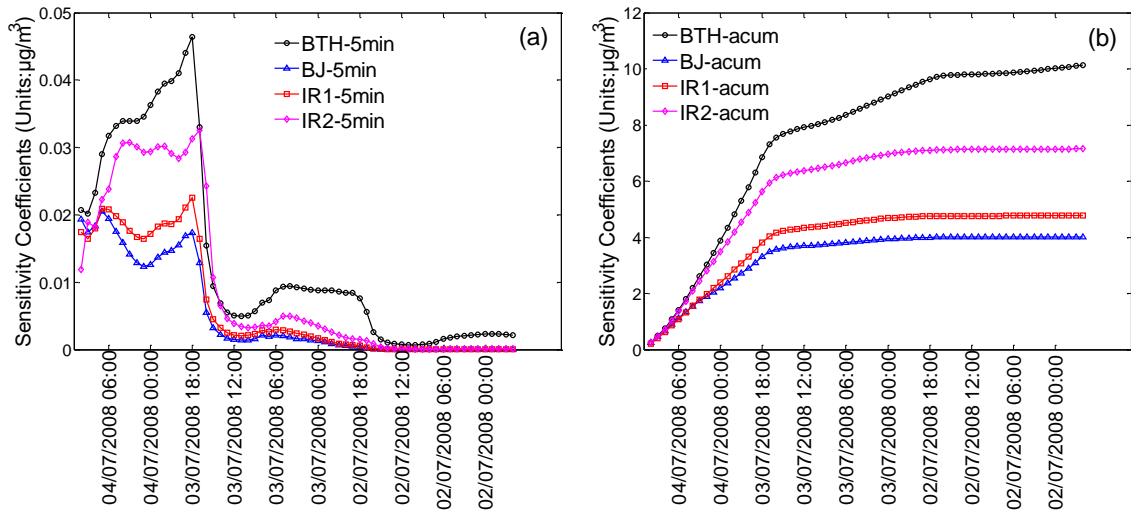
(a)-(e) are 1 h, 6 h, 11 h, 16 h, 21 h cumulative sensitivity coefficients

(f)-(g) are 24 h, 48 h cumulative coefficients, and (h) is the last backward simulation time step.



1
2
3
4
5

Figure 7. Different influential regions
 BTH: Red dashed frame; InR-1: Blue dashed frame;
 InR-2: Pinkish red solid frame; Object Region: yellow shadow



1
2
3

Figure 8. (a) Sensitivity coefficients at each 5-min integration time step along inverse time sequence; (b) Cumulative sensitivity coefficients along inverse time series.